Science Arts & Métiers (SAM)

is an open access repository that collects the work of Arts et Métiers ParisTech researchers and makes it freely available over the web where possible.

This is an author-deposited version published in: http://sam.ensam.eu
Handle ID: .http://hdl.handle.net/10985/8554

To cite this version :

Any correspondence concerning this service should be sent to the repository Administrator : archiveouverte@ensam.eu

An analysis of the elastic properties of a porous aluminium oxide film by means of indentation techniques

L. Hemmouche [a], D. Chicot [b,*], A. Amrouche [c], A. Iost [d], M.A. Belouchrani [a], X. Decoopman [b], G. Louis [e], E.S. Puchi-Cabrera [b,f,g]

[a] *Laboratoire Génie des Matériaux, Ecole Militaire Polytechniques, BP17C Bordj El Bahri, Alger, Algeria*
[b] *Laboratoire de Mécanique de Lille, LML, UMR 8107, USTLille, IUT A de LILLE I – Département GMP, BP 90179, 59 653 Villeneuve d'Ascq Cedex, France*
[c] *Laboratoire de Génie Civil et géo-Environnement LGCgE, EA 4515, Faculté des Sciences Appliquées FSA Béthune, Université d'Artois, France*
[d] *Arts et Métiers ParisTech, MSMP, 8, Boulevard Louis XIV, 59000 Lille Cedex, France*
[e] *EMDouai, MPE-GCE, F-59500 Douai, France*
[f] *School of Metallurgical Engineering and Materials Science, Faculty of Engineering, Universidad Central de Venezuela, Postal Address 47885, Los Chaguaramos, Caracas 1041, Venezuela*
[g] *Venezuelan National Academy for Engineering and Habitat, Palacio de las Academias, Postal Address 1723, Caracas 1010, Venezuela*

ARTICLE INFO

ABSTRACT

The elastic modulus of thin films can be directly determined by instrumented indentation when the indenter penetration does not exceed a fraction of the film thickness, depending on the mechanical properties of both film and substrate. When it is not possible, application of models for separating the contribution of the substrate is necessary. In this work, the robustness of several models is analyzed in the case of the elastic modulus determination of a porous aluminium oxide film produced by anodization of an aluminium alloy. Instrumented indentation tests employing a Berkovich indenter were performed at a nanometric scale, which allowed a direct determination of the film elastic modulus, whose value was found to be approximately 11 GPa. However, at a micrometric scale the elastic modulus tends toward the value corresponding to the substrate, of approximately 73 GPa. The objective of the present work is to apply different models for testing their consistency over the complete set of indentation data obtained from both classical tests in microindentation and the continuous stiffness measurement mode in nanoindentation. This approach shows the continuity between the two scales of measurement thus allowing a better representation of the elastic modulus variation between two limits corresponding to the substrate and film elastic moduli. Gao's function proved to be the best to represent the elastic modulus variation.

1. Introduction

Aluminium and its alloys have a natural surface heterogeneous oxide film, which is not enough corrosion resistant for many applications [1]. In these conditions, an anodising treatment leading to the formation of a more corrosion resistant thin film is used. The anodising treatment is usually performed in sulphuric acid solutions, giving rise to a porous structure consisting in hexagonal columnar cells like a honeycomb. Each cell consists of a central pore surrounded by alumina walls having both 10–20 nm in dimension. The cells grow normally to the surface of the aluminium substrate, which is separated from the cells by a thin barrier layer of 15 nm of thickness [1]. The structure of such an anodized material has been largely studied [1,2], but only few investigations on the

mechanical properties of the porous oxide film have been reported in the past [3,4].

From the investigation of the performance of coated materials it has been determined that the elastic modulus of the film is an important parameter [5–7]. One of the most suitable techniques for determining its value is the instrumented indentation tests by employing the methodology of Oliver and Pharr [8]. The choice of the scale of measurement, *i.e.* nanoindentation and/or microindentation, mainly resides in the nature (*global mechanical properties*, *heterogeneity*, *and presence of porosity…*) and the geometrical parameters (*thickness*, *roughness*, *and pores size…*) of the film. Nevertheless, a direct determination of the elastic modulus is possible by means of nanoindentation when the indenter displacement is less than a limiting value depending on the mechanical properties of the film and of the substrate. This criterion is usually defined in terms of critical ratio of coating thickness to indentation depth. Sun et al. [9] show that this critical ratio is a function of the yield strength ratio and also that it depends on the tip radius. This

* Corresponding author. Tel.: +33 359 572 852; fax: +33 320 677 321.
E-mail address: didier.chicot@univ-lille1.fr (D. Chicot).

critical ratio is around 1% for a hard film on soft substrate [10,11] but this value can reach up to 20% for a soft film on hard substrate [12,13]. Consequently, a direct determination can be unachievable for very thin films or in microindentation due to the range of applied loads which are not low enough to only affect the film behaviour. In these conditions, models are required for separating the contributions of the film and of the substrate from the measured or, often called, composite reduced modulus. These models have been formerly developed for analysing nanoindentation data by Gao et al. [14], Menčik et al. [15], Perriot and Barthel [16], Antunes et al. [17], Doerner and Nix [18] and Bec et al. [19] on the basis of the best fit of the elastic modulus variation as a function of the indenter displacement, film thickness and some adjusting parameters.

In order to analyze their reliability, all these models were applied in this work on indentation data ranging from nanoindentation to microindentation. For a sound discussion, these models must be applied on proper indentation data which are obtained after calibration of the instrument principally depending on the indentation mode and on the scale of measurement. Usually, the calibration must consider two aspects which can be analyzed separately: (*i*) the rounded-tip-effect on the contact area calculation and (*ii*) the determination of the frame compliance of the instrument/specimen couple. For the contact area calibration, Oliver and Pharr [8] suggested the use of a complex iteration function, which is justified in nanoindentation for the first nanometres of the indenter penetration, typically lower than 200 nm. For higher penetration depths, the correction introduced by Troyon and Huang [20], which consists in adding a constant value to the indenter displacement is enough precise regarding the magnitude of displacements in microindentation.

On the other hand, the frame compliance is considered to have a constant value in nanoindentation, whereas Chicot et al. [21] have shown that, in microindentation, the compliance term depends on the specimen mounting, shape and nature of the sample and testing conditions. Consequently, the frame compliance does not have a constant value for relative high loads and its value must be taken into account for each set of indentation data analyses. For this reason, Tricoteaux et al. [5] developed a model valuable for microindentation experiments, taking into account explicitly the frame compliance [22].

However, in the case of porous film the porosity is a very important parameter which can have a considerable influence on the elastic properties of the film and, consequently, on its elastic modulus value. The relationship between porosity and elastic modulus has been already proposed by Jernot et al. [23] who have connected the elastic modulus of a porous material to the massive one for sintered materials. This model has been modified by Tancret et al. [24] to take into account the size of the pores by separating the role of macro and microporosity. As an example for determining the elastic modulus of a microporous beta-TCP bioceramic, the model of Jernot et al. [23] has been successfully applied by Tricoteaux et al. [25] by neglecting the influence of the macroporosity. From a mathematical point of view, this model relates the elastic modulus of the porous material to the elastic modulus of the massive one, the degree of porosity and the number of grain boundaries connections.

In the present paper, the elastic modulus of a porous aluminium oxide film is determined by means of the instrumented indentation techniques at nano and micrometric scales. In nanoindentation, the continuous stiffness measurement mode is used to plot the elastic modulus as a function of the indenter displacement. In microindentation, the elastic modulus is determined by analyzing the unloading part of a load–depth curve. In this case, a unique value for the elastic modulus is obtained from each indentation curve. Both in nano and in microindentation, the same Berkovich indenter type is used. For analysing the load–displacement curve, the models of Oliver and Pharr [8] and Loubet et al. [26–28] are applied to take into account the deformation around the indent, sinking-in or piling-up, respectively. Indeed, this differentiation of the deformation mode is necessary since it affects the contact depth calculation and consequently, the contact area calculation. Afterwards, all the models are critically applied for determining the elastic modulus of the porous film and the porosity effect is studied by using the model of Jernot et al. [23]. For the tested material, the porosity of the film is associated to the presence of the pores inside the cells. Since the pores have a regular shape, the model of Jernot et al. [23] can be validly applied to compare the elastic modulus of the porous film to that of the massive aluminium oxide [3,4,29].

2. Experimental details

2.1. Material preparation

The experiments were conducted employing samples of a commercial 2017A-T4 aluminium alloy provided as sheet, whose chemical composition is given in Table 1. The metallurgical state T4 indicates that the material was solution treated at 500 °C during 50 min and water quenched at a temperature less than 40 °C. Following this heat treatment, the material was naturally aged for 4 days. After that, the specimens were degreased in an aqueous solution of sodium trisodiumphosphate Na_3PO_4 (60 g/l), sodium carbonate Na_2CO_3 (30 g/l) and sodium dodecylsulphate $C_{12}H_{25}NaO_4S$ (1.5 g/l) at 65 °C for 2 min, followed by rinsing with demineralised water. Then, pickling was done during a period of 5 min at 65 °C in an alkaline bath (10 g/l of NaOH) and neutralized in a sulphuric/chromic mixture (H_2SO_4: 180 ml/l, Cr_2O_3: 60 g/l) for 10 min at 65 °C. Finally, the specimens were anodized during 30 min in an aqueous solution of 180 g/l H_2SO_4 at 20 °C under a current of 1.5 A/dm^2. After anodizing, specimens were washed in distilled water and sealed in boiling water for 30 min at 96 °C.

Fig. 1a shows the scanning electronic microscopy (SEM) observation of the surface of the anodic oxide layer formed on 2017A-T4 aluminium alloy. This figure shows the grain boundaries (*white lines*) which results of the epitaxial growth of the oxides from each grain of the aluminium alloy substrate. Fig. 1b shows at a higher magnification the droplets of aluminium hydroxide which have grown at the surface of the aluminium oxide cells. The presence of the droplets hinders the visualization of the pores inside the cells. These droplets are the natural result of the sealing in boiling water for 30 min at 96 °C after anodization.

Fig. 2 illustrates a cross section of the film obtained after fracture by fatigue of an anodized sample. This figure shows that the mean value of the oxide film thickness is close to 12.5 ± 1.5 μm. This relative high standard deviation is due to the initial roughness of the sample before anodization. Note that in the following, the influence of the underlayer located between the substrate and the aluminium oxide film, having 15 nm of thickness, is neglected in the elastic modulus analysis. This approach is possible due to its relatively low thickness compared to that of the film.

Table 1
Chemical composition of 2017A-T4 aluminium alloy (wt%).

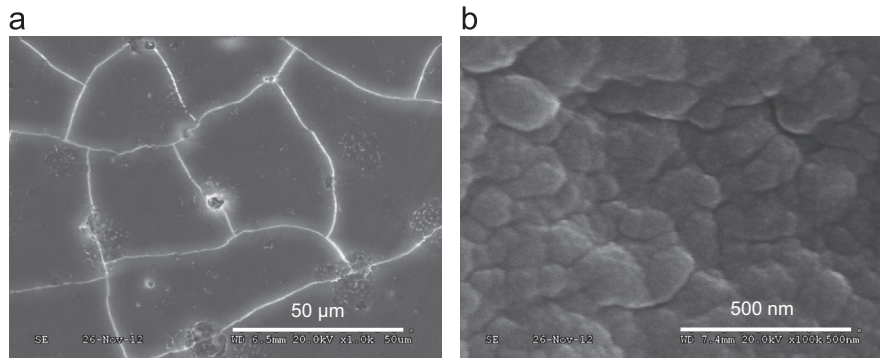| Element	Si	Cu	Ni	Fe	Zn	Mg	Mn	Cr	Ti	Al
wt%	0.57	4.19	0.07	0.47	0.01	0.61	0.29	0.04	0.04	Bal.

Fig. 1. Top-surface of the aluminium oxide film after anodization, (a) at ×1.0k and (b) at ×100k.
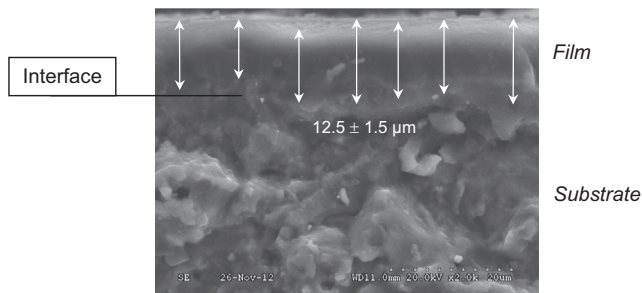

Fig. 2. Cross-section of aluminium oxide film after anodization.

Fig. 3. Load–displacement curves obtained by CSM mode in nanoindentation (a) and by classical loading mode in microindentation (b).

2.2. Indentation experiments

Nanoindentation experiments have been performed with a Nano Indenter XP™ (MTS Nano Instruments) employing a Berkovich diamond indenter. The anodized sample is fixed on a metallic support using the heat softening glue crystalbond 509. 25 indentation tests have been conducted randomly at the surface of the material with the same indentation testing conditions. The maximum indentation depth reached by the indenter was fixed at 2000 nm and the strain rate was equal to $0.05\ \text{s}^{-1}$. The instrument was operated in the continuous stiffness measurement (CSM) mode allowing the calculation of the elastic modulus continuously during the indentation loading. The harmonic displacement was 2 nm and the frequency was 45 Hz.

Microindentation experiments were carried out with a micro-hardness CSM 2-107 Tester equipped with a Berkovich diamond indenter. The load range of the instrument is from 0.1 to 20 N. The load resolution is given for 100 μN and the depth resolution for 0.3 nm, these values being provided by the CSM Instruments Group. Twenty five indentation tests were performed in this range of loads. The values of the loading and unloading rates (expressed in mN/min) were set at twice the value of the maximum applied load in mN, according to the rule proposed by Quinn et al. [30].

A dwell-time of 15 s was imposed according to the standard indentation test procedure ASTM E92 and E384-10e2. Note that the CSM mode is not available on the micro-hardness tester. As a result, the reduced elastic modulus is only calculated from the unloading part of the load–displacement curve. As an example, Fig. 3 shows typical load–displacement curves obtained in nano (Fig. 3a) and in microindentation (Fig. 3b).

In nanoindentation, pop-in events representing an increase in-depth at constant load are regularly observed for applied loads ranging between 10 and 30 mN. This abrupt change during loading can be connected to two phenomena: (1) the transition regime from elastic to elasto-plastic deformation of the material [31] or (2) the fracture of the oxide film due to the indentation stress intensity and
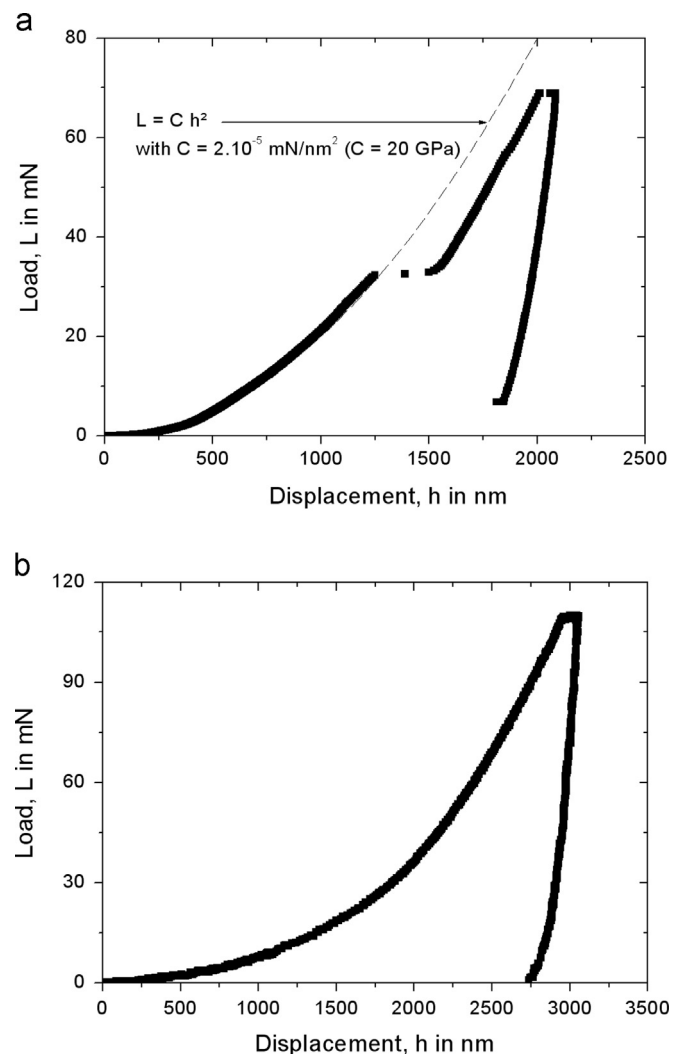
the brittleness of the film [32–34]. In case 1, Hertz's theory represented by the power law: $L=Kh^{3/2}$, where K is a parameter related to the elastic modulus, must be verified before the pop-in event. In practice, the exponent is found to be equal to 2 (Fig. 3a) thus indicating that the pop-in event is due to the fracture of the aluminium oxide cells. This observation is confirmed by the fact that the indenter penetration related to the pop-in event (1250 nm visible on Fig. 3a) equals to 10% of the film thickness (12.5 μm),
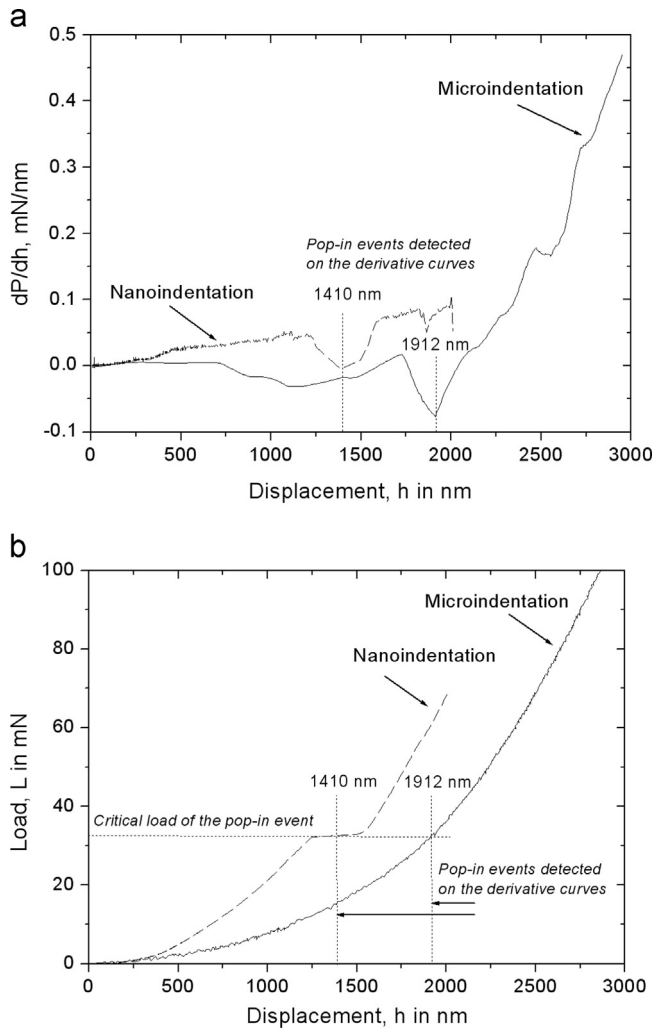
Fig. 4. Pop-in events observed on (a) the loading curves and (b) the derivative loadings curves both in nano and microindentation.

which corresponds to the interaction of the plastic zone with the substrate as it was already observed by Chechenin et al. [32]. On the other hand, it is noticeable that such pop-in events are not apparently observed in microindentation when using higher loads and classical loading rate conditions (Fig. 3b). However, it is suggested that the detection of the physical phenomenon can be conducted by analyzing the derivative of the loadings curves, as shown in Fig. 4a. For this purpose, the P–h data is fitted to a two-dimensional cubic spline with cubic ends. The resulting vector becomes the argument of an interpolation function, which can then be derived at every experimental data point. This figure clearly shows that the same phenomenon is observed in microindentation, but at a higher penetration depth, i.e. 1912 nm compared to 1410 nm observed in nanoindentation.

It is important to note that the corresponding applied loads of these pop-in events, which are reported in Fig. 4b, have the same value in both cases close to 32 mN. As a result, the extent of the pop-in event is clearly much more reduced in microindentation as compared to that in nanoindentation. These differences in the penetration depths and the extents of the pop-in events can be explained in terms of loading conditions. Indeed, the CSM mode in nanoindentation is similar to a dynamic loading under very low load-amplitudes, whereas in microindentation it is a continuous loading. It is assumed that the CSM mode accentuates the pop-in event and the delamination of the interface.

3. Instrumented indentation test: brief theoretical background

3.1. Indentation on massive materials

Instrumented indentation is a non-destructive method used to determine the mechanical properties of massive materials by analysing the load-displacement curve. The elastic modulus is deduced from the analysis of the unloading part of the (L–h) curve using initially the methodology of Oliver and Pharr [8]. The authors proposed the determination of the reduced modulus, E^*, from the computation of the contact area, A_C, and the compliance term of the sample which corresponds to the inverse of the unloading slope calculated at the maximum indentation depth, i. e. $C = (dh/dL)_{h=hmax}$, as follows:

$$E^* = \frac{\sqrt{\pi}}{2\beta\gamma} \frac{1}{\sqrt{A_C}} \frac{1}{(C - C_f)} \tag{1}$$

where C_f is the frame compliance of the instrument and β and γ two corrective factors. A_C is the projected contact area and E^* is defined as

$$\frac{1}{E^*} = \frac{1 - v^2}{E} + \frac{1 - v_i^2}{E_i} \tag{2}$$

where E, ν and E_i, ν_i represent Young's modulus and Poisson's ratio of the material and the indenter, respectively. For the diamond of the Berkovich indenter, the elastic modulus and the Poisson's ratio are 1140 GPa and 0.07, respectively [35].

The correction factor β is linked to the indenter geometry. By means of a three-dimensional simulation of a sharp indentation, β takes the value of 1.05 which is almost independent on the material [36]. The second correction factor γ introduced by Hay et al. [37] only depends on the Poisson's ratio as follows:

$$\gamma = \pi \frac{((\pi/4) + 0.1548((1-2v)/(4(1-v)))\cot\psi)}{((\pi/2) - 0.8312((1-2v)/(4(1-v)))\cot\psi)^2} \tag{3}$$

where $\psi = 70.3°$ represents the half-angle of the effective conical indenter.

Poisson's ratio of a massive aluminium oxide is given close to 0.21. Asmani et al. [38] showed that the Poisson's ratio is slightly affected by the fraction of porosity. For example, the authors give a variation between 0.24 and 0.20 for the Poisson's ratio when the porosity varies between 1% and 25%, respectively. In addition, Ko et al. [39] who studied the mechanical properties of a porous anodic alumina structure, advanced that the anisotropy is not accounted for the indentation method. According to this assumption, these authors have considered the constant value of 0.22 for the Poisson's ratio for the porous material, which is the same for the massive one. Finally as a result, a mean value of 0.2 for the Poisson's ratio is considered in the following for the calculation of the elastic modulus of the aluminium oxide film.

Moreover for a perfect Berkovich indenter, the projected contact area, A_C, is directly connected to the contact depth, h_c:

$$A_C = 24.56 h_c^2 \tag{4}$$

Unfortunately, the indenter tip is never perfect and its bluntness must be taken into account for accurate measurements. Within this objective, a variety of models describing the contact area function have been developed [20,40–47]. In nanoindentation, the complex area function expressing the contact area as a function of the contact indenter displacement is probably the most used:

$$A_C = 24.5 h_c^2 + C_1 h_c^1 + C_2 h_c^{1/2} + C_3 h_c^{1/4} + ... + C_8 h_c^{1/128} \tag{5}$$

where C_1 through C_8 are constants. The leading term describes a perfect conical indenter; the other additional terms describe deviations from the conical geometry due to blunting at the tip. For the indenter used in this work, $C_1 = 540$ nm^{-1}, $C_2 = 2882$ nm$^{-1/2}$, $C_3 = -4285$ nm$^{-1/4}$ and $C_4 = -894$ nm$^{-1/8}$. The others coefficients have been neglected for this calibration.

However, such a calibration procedure is not possible in microindentation. In this case, Troyon and Huang [20] proposed a simple model describing well-enough the actual contact area for indenter displacements higher than typically 200 nm. This methodology simply consists in adding a constant term, h_b, to the contact depth into the contact area calculation. The additional term represents the truncation length of the indenter tip-defect and the contact area function is then rewritten:

$$A_C = 24.5(h_c + h_b)^2 \tag{6}$$

Additionally, the calculation of the contact depth depends on the deformation mode around the indent. Indeed in presence of sinking-in, the method of Oliver and Pharr [8] is well-adapted and the contact depth is calculated from the maximum indentation depth, the maximum applied load and the compliance of the instrument as follows:

$$h_c = h_m - \varepsilon C L_m \tag{7}$$

where ε is a factor depending on the geometry of the indenter shape. $\varepsilon = 1$ for a flat punch indenter, 0.72 for a conical indenter and 0.75 for a spherical/paraboloïd indenter. In practice, its value is found to vary between 0.72 and 0.78, but for simplicity, ε will be taken as a constant value equal to 0.75.

When piling-up is observed at the surface of the indented material around the indent, the methodology of Oliver and Pharr underestimates the actual indentation depth. For this reason, Loubet et al. [26–28] suggested the computation of the contact depth by means of the following expression:

$$h_c = \alpha(h_m - C L_m) \tag{8}$$

where α is a constant equal to 1.2.

3.2. Indentation on thin films

When determining the mechanical properties of a coated system, especially in the case in which these involve very thin films, the reduced modulus calculated from Eq. (1) corresponds to a composite modulus, which takes into account the influences of both film and substrate. It is acknowledged that for a hard film deposited onto a soft substrate the presence of the latter becomes important as soon as the indenter displacement is higher than 1% of the film thickness [10,11], whereas this critical ratio can be around 20% for a soft film deposited onto a hard substrate [12,13]. For these reasons, application of different models for separating the contributions of the film and substrate is required.

The different models developed for nanoindentation [14–19] express the relative variation of the composite reduced elastic modulus compared to that of the substrate and of the film, as a function of the indenter displacement to thickness ratio. One can notice that, in these models, the fact that a direct determination is possible for very low indenter displacements is usually neglected. We will see hereafter that such an approximation can lead to a wrong estimation of the predicted elastic modulus value, the gap between the true and the predicted values increasing with this percentage.

From a general point of view, the deformation of the substrate is very small for the lowest loads and the system behaves globally like the film, whereas for higher loads the system behaves more like the substrate. When the indentation depth increases, the composite reduced elastic modulus changes gradually from the first limit, E_F^* (for very low loads), to the second limit, E_S^* (for higher loads). In the proposed models, the composite modulus, E_C^*, is expressed as a function of the substrate reduced modulus, E_S^*, and the film reduced modulus, E_F^*.

The different models are summarized in Table 2 where the composite modulus is expressed as a combination of those of the substrate and film in relation to the indenter displacement, h, to the film thickness, t, and different empirical parameters, α_i and x. Note that all the models express a relative variation of the elastic modulus or a function of its reciprocal. In Table 2, the empirical weight parameter Φ, usually called the Gao's function, was proposed by Gao et al. [14], which is expressed as

$$\Phi = \frac{2}{\pi}\arctan\xi + \frac{1}{2\pi(1-v)}\left[(1-2v)\xi\ln\left(\frac{1+\xi^2}{\xi^2}\right) - \frac{\xi}{1+\xi^2}\right] \tag{9}$$

where, for a Berkovich indenter, ξ equals to $(t/[h\tan\psi])$ and ψ is the effective semi-angle of an equivalent conical indenter ($=70.3°$).

Gao's function has already been applied by numerous authors [48–53]. Unfortunately, the form of this function differs according to the authors who employed it. Mencik et al. [48], Hay and Crawford [53] and Sawa et al. [49] confirmed the general form of Eq. (9) even if the parameter ξ has been associated to different expressions. Chen and Vlassak [51] have considered a negative sign in the last ratio in Eq. (9), i.e. $\xi/(1-\xi^2)$ instead of $\xi/(1+\xi^2)$ which leads obviously to a discontinuity of Gao's function when ξ equals 1. For Malzbender et al. [50], the difference comes from the first term where the ARCTAN function is in the denominator. For Fernandes et al. [52], the last term in Eq. (9) is considered inside the logarithmic function, that is to say, within the same brackets. As a result, particular attention must be paid when applying Gao′s function found in the literature.

In the model of Perriot and Barthel [16], the fitting parameters are connected to the film to substrate elastic moduli ratio thus limiting its ability to adequately represent the elastic modulus variation. That is probably why Korsunsky and Constantinescu [54] kept the free-dependence these two fitting parameters in WF$_3$. Note that these authors have based their model on their own model developed for the hardness determination of thin film which leads to the same expression given by Perriot and Barthel [16]. On the other hand, the original model proposed by Bec et al. [19] does not involve any fitting parameter but in its present form it does not permit a best fitting of the experimental data. However, this model can be extended since it has been developed for a rigid cylindrical punch. To take into account the difference between a sharp indenter and a cylindrical one, called anvil effect by the

Table 2
Different weight functions (WF) available in literature using relative variation of the elastic modulus (a) or of the reciprocal elastic modulus (b).

(a) Weight functions with elastic modulus	
Gao et al. [14]	Mencik et al. [15]
$WF_1 = \frac{\|E_C^* - E_S^*\|}{\|E_F^* - E_S^*\|} = \Phi$	$WF_2 = \frac{\|E_C^* - E_S^*\|}{\|E_F^* - E_S^*\|} = e^{(-\alpha_2(h/t))}$
Perriot and Barthel [16]	Antunes et al. [17]
$WF_3 = \frac{\|E_C^* - E_S^*\|}{\|E_F^* - E_S^*\|} = \frac{1}{1+\alpha_3(h/t)^x}$	$WF_4 = \frac{\|E_C^* - E_F^*\|}{\|E_F^* - E_S^*\|} = e^{(-\alpha_4(t/h))}$
(b) Weight functions with reciprocal elastic modulus	

Doerner and Nix [18]	Mencik et al. [15]
$WF_5 = \frac{\|1/E_C^* - 1/E_F^*\|}{\|1/E_S^* - 1/E_F^*\|} = e^{(-\alpha_5(t/h))}$	$WF_6 = \frac{\|1/E_C^* - 1/E_F^*\|}{\|1/E_F^* - 1/E_S^*\|} = e^{(-\alpha_6(h/t))}$
Bec et al. [19]	Antunes et al. [17]
$WF_7 = \frac{\|1/E_C^* - 1/E_S^*\|}{\|1/E_F^* - 1/E_S^*\|} = \frac{1}{1+(\pi/2)\tan\psi(h/(\alpha_7(t-h)))}$	$WF_8 = \frac{\|1/E_C^* - 1/E_S^*\|}{\|1/E_F^* - 1/E_S^*\|} = \Phi$

authors [54], we propose the use of the relation indicated in Table 2 where the term $\alpha_7(t-h)$ replaces the original term t.

In microindentation and due to the role of the frame compliance on the indentation data analysis, Tricoteaux et al. [5] proposed a model where the frame compliance is explicitly taken into account. By analogy, this model is very similar to that earlier proposed by Korsunsky and Constantinescu [54] if the frame compliance is neglected:

$$\frac{1}{S_C} = P_0 + \frac{P_1}{h} + \frac{P_2}{h(1 + P_3 h^2)} \tag{10}$$

with

$$P_0 = C_f, \quad P_1 = \frac{1}{2\beta}\sqrt{\frac{\pi}{24,5}}\frac{1}{\gamma_s E_s^*},$$
$$P_2 = \left(\frac{1}{2\beta}\sqrt{\frac{\pi}{24,5}}\right)\left(\frac{1}{\gamma_f E_f^*} - \frac{1}{\gamma_s E_s^*}\right) \text{ and } P_3 = k'$$

and where P_1 depends only on the elastic modulus of the substrate whereas P_2 depends on both substrate and film elastic moduli. P_3 is a fitting parameter.

4. Results and discussion

To determine the elastic modulus of a film using nanoindentation and/or microindentation tests, different aspects must be carefully studied regarding the terms involved in Eq. (1). Since the frame compliance of the instrument, C_f, depends on the sample/instrument couple and on the indentation test conditions in microindentation [21,55, 56], its value must be determined for each set of indentation tests. For a coated system, the frame compliance can be determined by employing the model of Tricoteaux et al. [5]. The value of C_f is then obtained by plotting the reduced elastic modulus versus the reciprocal indenter displacement; C_f is then obtained when the x-coordinate equals zero.

In this work, C_f has a negative value of -0.0105 μm/N. Such a negative value can be surprising but its variation is complex and the origins of such variation are large, like the frame compliance of the instrument, the mounting system, presence of glue or epoxy resin, indenter fixing, testing conditions, roughness, etc. [21,56]. On the other hand, its value can be also greatly affected by the scatter of the measurements of the composite reduced elastic modulus due to the substrate roughness and the variation of the film thickness. Given the large amount of parameters which can be involved, the exact dependency of the frame-compliance value is not yet well-known. Independently, it is important to note that the correction of the contact area function is not related to the determination of the frame compliance since the latter is determined when the loads tend to an infinite value, where the different corrections on the contact area become insignificant.

In a second step, knowledge of the deformation mode around the indent is necessary to select the methodology which must be applied, *i.e.* the methodology of Oliver and Pharr [8] for sinking-in or the methodology of Loubet et al. [26–28] for piling-up. These two methodologies mainly differ in the calculation of the contact indenter displacement (see Eqs. (7) and (8)). Independently of that, the truncation length of the indenter tip-defect, h_b, is necessary to calculate the contact area function in microindentation by applying Eq. (6). To estimate its value, a field emission SEM from HITACHI, type S-4300 SE/N, was employed to observe the Berkovich indenter tip used in the microhardness tester. This microscope allows working with acceleration voltages between 0.5 and 30 kW, which can lead to a resolution of 1.5 nm, corresponding to an enlargement of $500,000 \times$ at a pressure of 10^{-6} Pa. As a result, h_b was found to be close to 50 nm, whereas the standard deviation is estimated around 10 nm.

Now, the two methodologies are applied to determine analytically the mode of calculation of the contact indenter displacement by comparing the value of the elastic modulus obtained for the highest applied loads to the value of 73 GPa corresponding to the theoretical value of the elastic modulus of the aluminium alloy 2017A.

This value of 73 GPa has been confirmed by Fernandez et al. [57] using ultrasonic techniques. The analysis is necessarily done in microindentation because the applied loads are sufficient enough to neglect the influence of the film. The elastic modulus of the coated system is calculated by means of Eq. (2) where the reduced elastic modulus, E^*, is obtained by applying Eq. (1). $C_f = -0.0105$ μm/N and the contact area function is calculated by Eq. (6), where $h_b = 50$ nm. The contact indenter displacement is then calculated by using Eq. (7) when considering the methodology of Oliver and Pharr [8] or by Eq. (8) for the methodology of Loubet et al. [26–28].

The corrective parameters are $\beta = 1.05$ and $\gamma = 1.09$, calculated taking into account the value of 0.2 for the Poisson's ratio of the film involved in Eq. (3). Fig. 5 represents the elastic modulus of the anodized material as a function of the indenter displacement when considering piling-up (opened circle) or sinking-in (black square) formation around the indent.

Fig. 5 shows that the methodology of Oliver and Pharr [8] is more appropriate to represent the variation of the elastic modulus of the coated system since the values of the composite elastic modulus calculated for the highest indenter displacements, or for the highest applied loads, tend toward 73 GPa corresponding to that of the substrate, whereas in the second case, the elastic modulus tends toward 63 GPa. As a consequence, the methodology of Oliver and Pharr is considered in the following.

However, it is clear on this figure that the number of elastic modulus data obtained for the lowest indenter displacements is not consistent enough for an accurate determination of the elastic modulus of the film. That is why nanoindentation experiments have been performed. Among the 25 experiments, a small number of curves are considered for representing the elastic modulus variation. Fig. 6 presents these curves obtained by the CSM mode between 0 and 2000 nm.

Fig. 6a shows the total range of the indenter displacements whereas Fig. 6b shows an enlargement of the results between 0 and 200 nm in order to visualize better the elastic modulus variation at the beginning of the nanoindentation experiments. Fig. 6 reveals an important scatter of the elastic modulus value which can be the result of the substrate roughness before growth of an epitaxial film and the
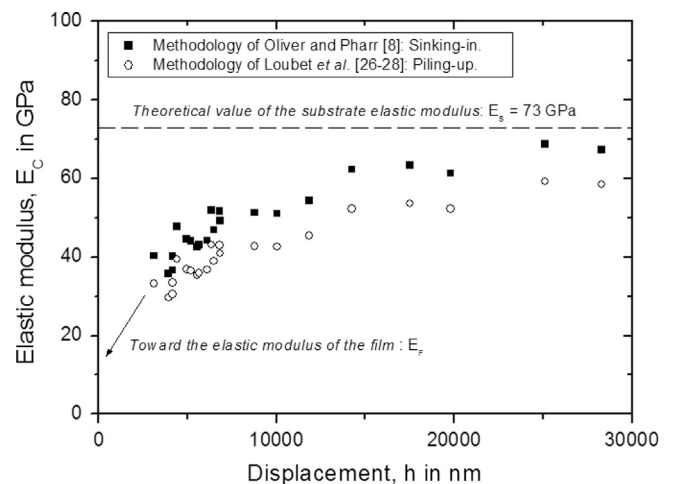
Fig. 5. Composite elastic modulus of the coated system determined by microindentation considering the methodologies of Oliver and Pharr [8] and Loubet et al. [26–28].
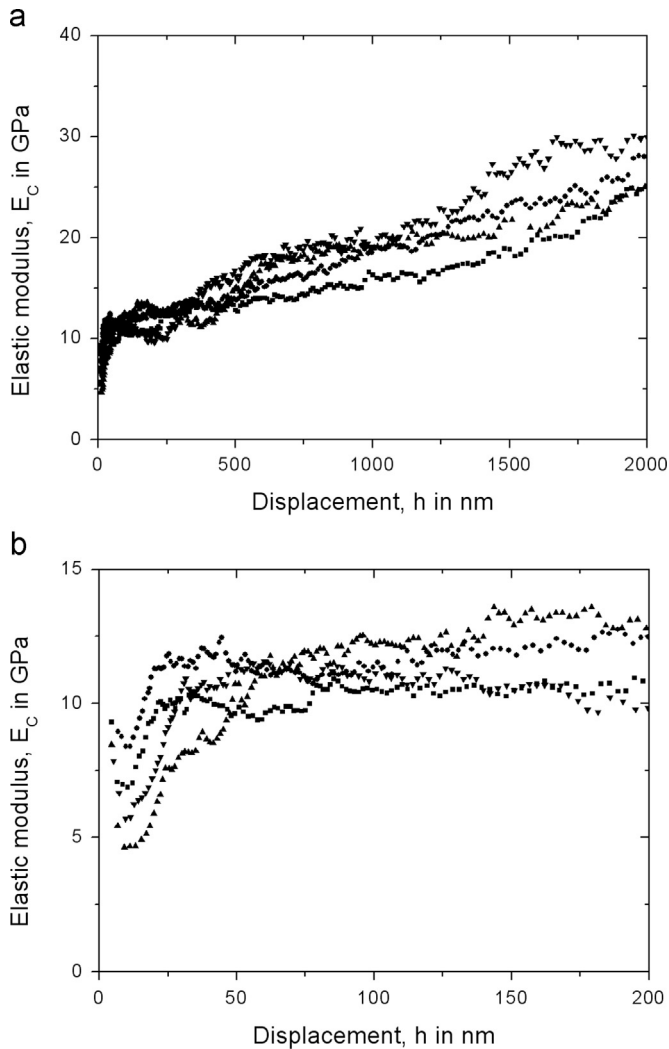
a

b

Fig. 6. Composite elastic modulus of the coated system determined by the CSM mode in nanoindentation and considering the methodology of Oliver and Pharr [8]. (a) Complete zone of measurement and (b) Enlargement of the graph (a).

Fig. 7. Reduced modulus of fused silica for the contact area calibration of the Berkovich indenter used in nanoindentation.

Fig. 8. Compilation of the composite elastic modulus deduced from nano and microindentation tests applied to the porous oxide film as a function of the relative indentation depth where the film thickness is of 12.5 μm.

discrepancy of the film thickness as it is visible in Fig. 2. However, Fig. 6a shows that the elastic modulus varies quasi continuously as a function of the indenter displacement and that the value of E_C reached at 2000 nm is very different to that of the substrate.

This observation confirms the need to apply different models for separating the contribution of the substrate from the measurement. However, Fig. 6b tends to show that the variation is quite constant over the 200 first nanometres. This value corresponds to the elastic modulus of the film. The variation, which can be observed in this range of displacement, is attributed to the porosity and the roughness visible in Fig. 1b. As a main result, a mean value of the elastic modulus of the film can be estimated, whose magnitude is $E_f = 11 \pm 1.5$ GPa. The decrease which is observed for the lowest values of the indenter displacements could be attributed to various causes, such as the roughness, the presence of pores or the influence of the tip defect. To have a sound discussion, we present in Fig. 7 the result obtained on fused silica for the contact area calibration using Eq. (5) due to Oliver and Pharr [8].

Fig. 7 confirms that the variations observed in Fig. 6 between 0 and 30 nm are due to the approximation of the contact area calibration in this range of indenter displacements. However, this also confirms that the elastic modulus measured between 30 and 200 nm which is quite constant must correspond to the elastic modulus of the film. This result indicates that the critical ratio of
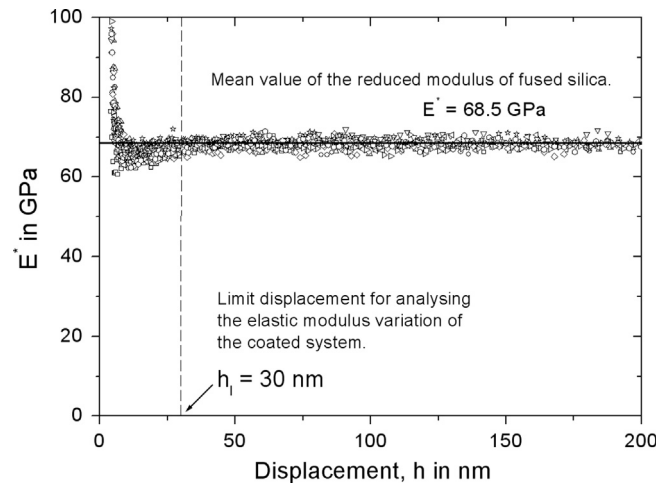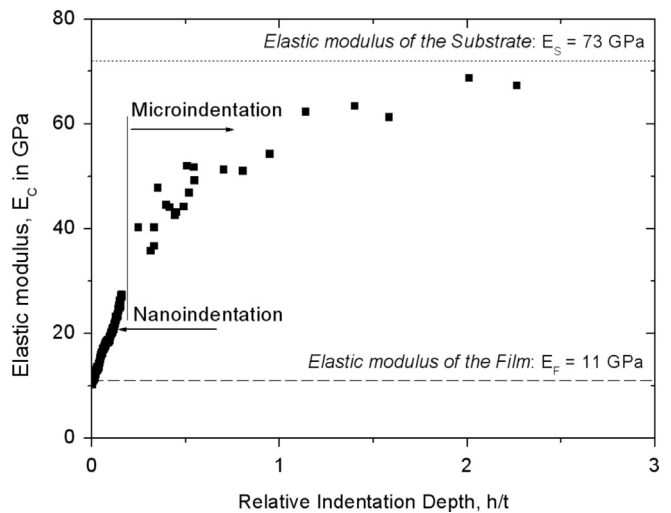
film thickness to indentation depth has not the constant value of 1% as usually admitted [10,11] but this value must be adjusted because the film thickness is around 12.5 μm as it can be seen in Fig. 2.

As a result, the elastic modulus of the porous aluminium oxide is equal to 11 GPa (Fig. 6b). Now and knowing the elastic modulus of the film, it is possible to test the robustness of the different models [3,14–19]. All the elastic modulus values obtained in nanoindentation (Fig. 6) and microindentation (Fig. 5) are plotted on the same graph (Fig. 8) as a function of the relative indentation depth. It is noticeable that, independently of the calculation mode of the elastic modulus in nano and in microindentation, it seems that all the indentation data can be represented by a unique curve thus allowing the conciliation between nano and microindentation with their specific methodologies.

Consequently, the different weight functions collected in Table 2 have been applied on the complete range of indentation data. The model of Tricoteaux et al. [5] has been applied for determining the frame compliance in microindentation. Table 3 collects the predictive values obtained for the elastic modulus of the film and of the substrate, as well as the values of the different fitting parameters involved in the weight functions presented in Table 2. Note that the deviations between the theoretical curve

Table 3
Predictive values for the elastic modulus of the film and of the substrate and values of the fitting parameters according to the weight functions presented in Table 2.

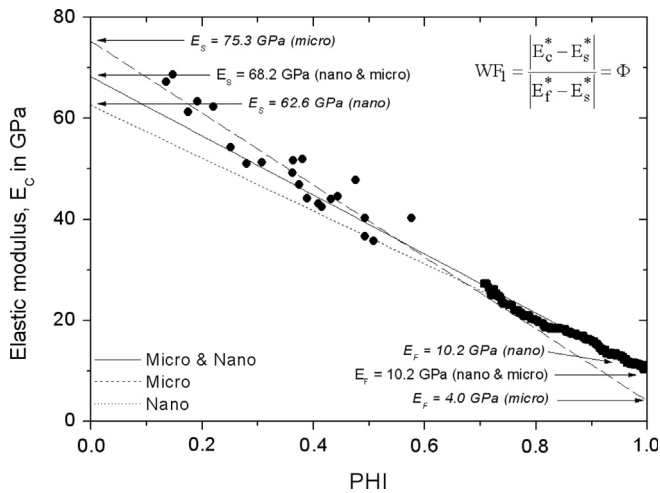|	WF$_1$	WF$_2$	WF$_3$	WF$_4$	WF$_5$	WF$_6$	WF$_7$
E_f (GPa)	9.7	10.1	10.6	10.1	11.1	10.5	10.2
E_s (GPa)	68.2	66.4	73.6	66.4	47.2	44.6	67.8
α_i		2.10	3.18	2.10	0.05	10.52	1/3
x			1.22				

Fig. 9. Model of Gao et al. [14] applied on the indentation data obtained from nano and microindentation tests performed on the porous aluminium oxide film.

and the experimental points were minimized by the least-square method in order to find the best set of parameters to predict the film and substrate elastic modulus.

From a general point of view, it appears that the models, which involve the reciprocal elastic modulus, WF$_5$–WF$_8$ except WF$_7$, lead to lower values for the elastic modulus prediction of the substrate; i.e. less than 50 GPa instead of 73 GPa given as the theoretical value. Additionally, WF$_8$ is not able to predict the elastic moduli. Indeed in this study, the representation of the weight function is not linear as a function of the parameter ϕ even if the tendencies at the two extreme limits converge toward the elastic moduli of the film and of the substrate.

Among other weight functions, we retained two models, i.e. the model of Gao et al. [14] (WF$_1$) where no fitting parameter has been introduced into the weight function and the model of Korsunsky and Constantinescu [54] which leads to the best prediction when comparing the predicted values to the theoretical value for the substrate and to the experimental value for the film obtained for the lowest indenter displacements in nanoindentation. However, some comments must be done concerning these two models.

Indeed, Fig. 9 presents the model of Gao et al. [14] applied on the complete range of indentation data. It is interesting to note that, independently of the mode of calculation, i.e. classical or CSM mode, all the values for the composite elastic modulus seem to be adequately represented by a unique straight line. The elastic modulus of the substrate is determined when Φ is null, whereas that of the film is obtained when this parameter equals 1. It is also interesting to note that the nanoindentation data are predominant in the fitting weight since more than 1000 data points have been obtained whereas only 25 indentation data points are obtained in microindentation.

This could explain the slight deviation which can be observed when ϕ tends toward zero, thus explaining the difference between the predicted value for the elastic modulus of the substrate,

68.2 GPa, and the theoretical one of 73 GPa. Note than when the model is applied separately on the microindentation data and on the nanoindentation data, the predicted values change. As it was expected, the elastic modulus of the substrate is well predicted by microindentation experiments whereas nanoindentation obviously leads to the best prediction of the elastic modulus of the film.

As a conclusion, nanoindentation can be logically employed for determining the elastic modulus of the film but it must be carefully interpreted for estimating the elastic modulus of the substrate when its value is unknown. In the same way, micro-indentation can be useful to advantageously complete the range of nanoindentation data, which allows a better prediction of the elastic modulus of the substrate. However depending on the elastic properties of the film and substrate and of the film thickness, it is very important to keep in mind that the difference between the predicted value by the Gao's function and the actual value can diverge to a great extent. In these conditions, Gao's function must be carefully applied in microindentation.

To estimate the deviation between the actual and the predicted values of the elastic modulus of the film, we represent in Fig. 10a schematic elastic modulus variation as a phi-function. The deviation noted ΔE equals to ($E_{fA} - E_{fP}$) where E_{fA} represents the actual elastic modulus of the film and E_{fP} its predicted value by the model. The amplitude of this deviation is connected to the total distance over which the substrate does not interfere into the elastic modulus measurement, that is to say when the indenter displacement is less than a given fraction of the film thickness defining h_{lim}, and to the ratio between the substrate and the film elastic moduli (E_f/E_s).

As an example, when the film thickness has a high value and when the two elastic moduli of the film and substrate are very different, the predicted value can be very different of the actual elastic modulus of the film. For the model of Korsunsky and Constantinescu [54], the problem which occurs is that the accuracy of the prediction greatly depends on the number of the experimental data. Indeed, Fig. 11 shows the representation of this model applied to the entire range of experimental data and on the nanoindentation and microindentation results taken separately. This figure confirms the need to take into account all the range of indentation data: (i) to correctly represent the elastic modulus variation and (ii) for an accurate determination of the elastic modulus of the film from microindentation and of the substrate from nanoindentation.
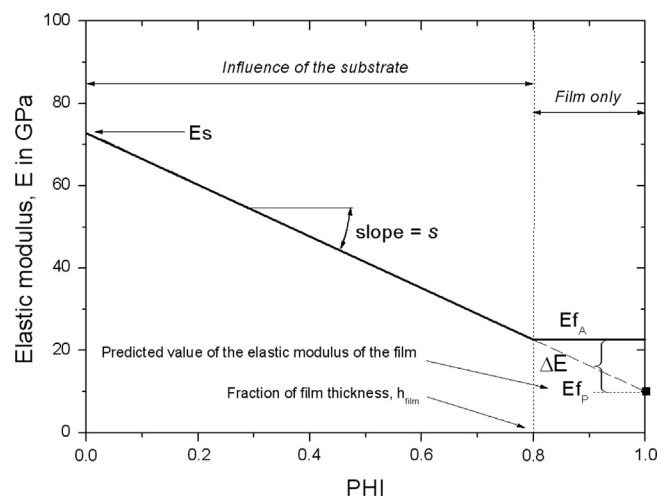

Fig. 10. Schematic representation of the composite elastic modulus versus a function depending on the indenter displacement, h, the film thickness, t, and a fitting parameter, α_i.
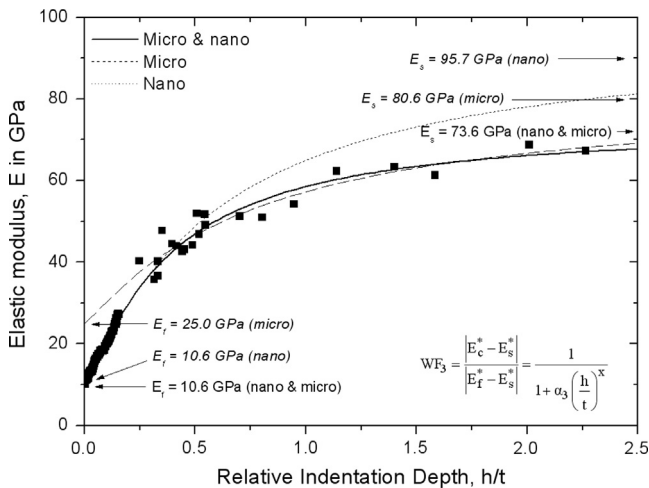
Fig. 11. Models of Perriot and Barthel [16] and Korsunsky and Constantinescu [53] applied on the indentation data obtained from nano and microindentation tests performed on the porous aluminium oxide film.

Additionally, to support the determination of the elastic modulus of the film by instrumented indentation, the elastic modulus is then discussed as a function of the porosity of the film. To introduce the influence of the porosity on the elastic modulus determination, the model of Jernot et al. [23] is applied. The mathematical expression is given by

$$E = E_0[N_C(1-p)-(N_C-1)(1-p)^{2/3}] \qquad (11)$$

where E_0 is the elastic modulus of the massive material, p is the volume fraction representative of the porosity degree and N_C the mean coordinate number.

Application of Eq. (11) requires the determination of the porosity, p, and the coordinate number, N_C, which depends both on the specific morphology of the layer obtained by anodization and the knowledge of the elastic modulus of the dense material, E_0. The porous layer is composed of hexagonal columnar cells [1] and, consequently, the coordinate number can be associated to the number of neighbours for these columns (6 in this study). On the other hand, Chechenin et al. [3] have determined by nanoindentation the elastic modulus of an aluminium oxide film obtained by anodizing oxidation.

In their work, the elastic modulus is close to 160 GPa which can be assimilated to E_O since no porosity is reported in the paper of Chechenin et al. [3] for the film. Application of Eq. (11) when E_f equals 11 GPa leads to 0.39 for p. This result is in a very good agreement with the work of Feliu et al. [1] who reported a volume fraction porosity of 39% obtained for a film formed by anodization performed in a sulphuric bath containing 180 g/l of H_2SO_4 at 20 °C and current density of 1.5 A dm^{-2} for 30 min which are the same conditions of treatment used in this work.

5. Conclusions

The determination of the elastic modulus of porous thin films poses some difficulties. In this work, it has been shown that the elastic modulus of the film can be determined by nanoindentation. However, for an accurate representation of the indentation data between the film and the substrate tendencies, association of nanoindentation and microindentation is required. For the porous aluminium oxide film, the model of Gao et al. gives an adequate representation of the indentation data, where only geometrical parameters linked to the size of the indent and to the film thickness are necessary. For a best determination of the elastic

modulus both of the film and of the substrate, the model of Korsunsky and Constantinescu is probably the more consistent. However, it requires a large number of indentation data values over all the range of loads applied. Finally, it has been found that for the elastic modulus of the porous film, $E_f = 11$ GPa and by using the model of Jernot et al., a porosity degree is found to be equal to 39%, which is in accordance with results presented in the literature. As a main conclusion, it has been shown that Gao's function is quite appropriate for representing the variation of the elastic modulus since it requires no fitting parameters, as well as the fact that it can be applied both to nanoindentation and microindentation data. However, some precautions should be taken, particularly regarding the influence of the substrate to film elastic modulus ratio and to the film thickness.

References

[1] S. Feliu, J.A. González, V. López, M.J. Bartolome, E. Escudero, E. Otero, Appl. Electrochem. 37 (2007) 1027–1037.
[2] J.P. Dasquet, D. Caillard, E. Conforto, J.P. Bonino, R. Bes, Thin Solid Films 371 (2000) 183–190.
[3] N.G. Chechenin, J. Bottiger, J.P. Krog, Thin Solid Films 304 (1997) 70–77.
[4] K. Koski, J. Hölsä, P. Juliet, Thin Solid Films 339 (1999) 240–248.
[5] A. Tricoteaux, G. Duarte, D. Chicot, E. Le Bourhis, E. Bemporad, J. Lesage, Mech. Mater. 42 (2010) 166–174.
[6] A. Leyland, A. Matthews, Wear 246 (2000) 1–11.
[7] J.C.A. Batista, C. Godoy, G. Pintaúde, A. Sinatora, A Matthews, Surf. Coat. Technol. 174–175 (2003) 891–898.
[8] W.C. Oliver, G.M. Pharr, J. Mater. Res. 7 (1992) 1564–1583.
[9] Y. Sun, T. Bell, S. Zheng, Thin Solid Films 258 (1995) 198–204.
[10] T. Chudoba, N. Schwarzer, F. Richter, Surf. Coat. Technol. 154 (2002) 140–151.
[11] F. Cleymand, O. Ferry, R. Kouitat, A. Billard, J. von Stebut, Surf. Coat. Technol. 200 (2005) 890–893.
[12] T. Ohmura, S. Matsuoka, K. Tanaka, T. Yoshida, Thin Solid Films 385 (2001) 198–204.
[13] Z.H. Xu, D. Rowcliffe, Thin Solid Films 447–448 (2004) 399–405.
[14] H. Gao, C.H. Chiu, J. Lee, Int. J. Solids Struct. 29 (1992) 2471–2492.
[15] J. Menčik, D. Munz, E. Quandt, E.R. Weppelmann, M.V. Swain, J. Mater. Res. 12 (1997) 2475–2484.
[16] A. Perriot, E. Barthel, J. Mater. Res. 19 (2004) 600–608.
[17] J.M. Antunes, J.V. Fernandes, N.A. Sakharova, M.C. Oliveira, L.F. Menezes, Int. J. Solids Struct. 44 (2007) 8313–8334.
[18] M.F. Doerner, W.D. Nix, J. Mater. Res. 1 (1986) 601–609.
[19] S. Bec, A. Tonck, J.L. Loubet, Philos. Mag. A 86 (2006) 5347–5358.
[20] M. Troyon, L. Huang, J. Mater. Res. 20 (2005) 610–617.
[21] D. Chicot, F. Roudet, A. Zaoui, G. Louis, V. Lepingle, Mater. Chem. Phys. 119 (2010) 75–81.
[22] D. Chicot, E.S. Puchi-Cabrera, R. Aumaitre, G. Bouscarrat, C. Dublanche-Tixier, F. Roudet, M.H. Staia, Thin Solid Films 522 (2012) 304–313.
[23] J.P. Jernot, M. Coster, J.L. Chermant, Phys. Status Solidi 72 (1982) 325–332.
[24] F. Tancret, J.M. Bouler, J. Chamousset, L.M. Minois, J. Eur. Ceram. Soc. 26 (2006) 3647–3656.
[25] A. Tricoteaux, E. Rguiti, D. Chicot, L. Boilet, M. Descamps, A. Leriche, J. Lesage, J. Eur. Ceram. Soc. 31 (2011) 1361–1369.
[26] J.L. Loubet, M. Bauer, A. Tonck, S. Bec, B. Gauthier-Manuel, NATO Advanced Study Institute Series E (1993) 429–447.
[27] S. Bec, A. Tonck, J.M. Georges, E. Georges, J.L. Loubet, Philos. Mag. A 74 (1996) 1061.
[28] G. Hochstetter, A. Jimenez, J.L. Loubet, Sci. Phys. B38 (1999) 681–692.
[29] P. Auerkari, Mechanical and physical properties of engineering alumina ceramics, VTT Tiedotteita – Meddelanden – Research Note 1792, Technical Research Centre of Finland (VTT), 1996, 26 pp.
[30] G.D. Quinn, P.L. Patel, I. Lloyd, J. Res. Natl. Inst. Stand. Technol. 107 (2002) 299–306.
[31] D. Lorenz, A. Zeckzer, U. Hilpert, P. Grau, H. Johansen, H.S. Leipner, Phys. Rev. B67 (2003) 172101.
[32] N.G. Chechenin, J. Bottiger, J.P. Krog, Thin Solid Films 261 (1995) 228–235.
[33] K.R. Morasch, D.F. Bahr, J. Mater. Res. 20 (2005) 1490–1497.
[34] Y. Gaillard, E. Jiménez-Piqué, F. Soldera, F. Mücklich, M. Anglada, Acta Mater. 56 (2008) 4206–4216.
[35] J.E. Field, R.H. Telling, The Young modulus and Poisson ratio of diamond. Research Note, Cavendish Laboratory, Cambridge, 1999.
[36] M. Dao, N. Chollacoop, K.J. Van Vliet, T.A. Venkatesh, S. Suresh, Acta Mater. 49 (2001) 3899–3918.
[37] J.C. Hay, A. Bolshakov, G.M. Pharr, J. Mater. Res. 14 (1999) 2296–2305.
[38] M. Asmani, C. Kermel, A. Leriche, M. Ourak, J. Eur. Ceram. Soc. 21 (2001) 1081–1086.
[39] S. Ko, D. Lee, S. Jee, H. Park, K. Lee, W. Hwang, Thin Solid Films 515 (2006) 1932–1937.

[40] K. Herrmann, N.M. Jennett, W. Wegener, J. Meneve, K. Hasche, R. Seemann, Thin Solids Films 377–378 (2000) 394–400.
[41] A. Krell, S. Schädlich, Mater. Sci. Eng. A 307 (2002) 172–181.
[42] J. Thurn, R.F. Cook, J. Mater. Res. 17 (2002) 1143–1146.
[43] J.M. Antunes, A. Cavaleiro, L.F. Menezes, M.I. Simoes, J.V. Fernandes, Surf. Coat. Technol. 149 (2002) 27–35.
[44] A.R. Franco Jr, G. Pintaude, A. Sinatora, C.E. Pinedo, A.P. Tschiptschin, Mater. Res. 7 (2004) 483–491.
[45] H. Bei, E.P. George, J.L. Hay, G.M. Pharr, Phys. Rev. Lett. 95 (2005) 045501.
[46] L.A. Berla, A.M. Allen, S.M. Han, W.D. Nix, J. Mater. Res. 25 (2010) 735–745.
[47] S. Liu, Y. Gu, H. Huang, Mater. Sci. Eng. A 528 (2011) 7948–7951.
[48] J. Menčik, E. Quandt, D. Munz, Thin Solid Films 287 (1996) 208–213.
[49] T. Sawa, Y. Akiyama, A. Shimamoto, K. Tanaka, J. Mater. Res. 14 (1999) 2228–2232.
[50] J. Malzbender, G. de With, J.M.J. den Toonder, Thin Solid Films 366 (2000) 139–149.
[51] X. Chen, J.J. Vlassak, J. Mater. Res. 16 (2001) 2974–2982.
[52] J.V. Fernandes, J.M. Antunes, N.A. Sakharova, M.C. Oliveira, L.F. Menezes, Philos. Mag. Lett. 90 (2010) 9–22.
[53] J. Hay, B. Crawford, J. Mater. Res. 26 (2011) 727–738.
[54] A.M. Korsunsky, A. Cosntantinescu, Thin Solid Films 517 (2009) 4835–4844.
[55] K. Demmou, S. Bec, J.L. Loubet, J.M. Martin, Tribol. Int. 39 (2006) 1558–1563.
[56] A.C. Fischer-Cripps, Surf. Coat. Technol. 200 (2006) 4153–4165.
[57] J.L. Fernandez, J.L. Dean, C. Trillo, A.F. Doval, Opt. Laser Eng. 45 (2007) 618–630.